Energy Transport by Thermocapillary Convection during Sessile-Water-Droplet Evaporation

H. Ghasemi and C. A. Ward*

Department of Mechanical and Industrial Engineering, Thermodynamics and Kinetics Laboratory, University of Toronto, 5 King's College Road, Toronto, Canada, M5S 3G8

(Received 14 June 2010; published 23 September 2010)

The energy transport mechanisms of a sessile-water droplet evaporating steadily while maintained on a Cu substrate are compared. Buoyancy-driven convection is eliminated, but thermal conduction and thermocapillary convection are active. The dominant mode varies along the interface. Although neglected in previous studies, near the three-phase line, thermocapillary convection is by far the larger mode of energy transport, and this is the region where most of the droplet evaporation occurs.

DOI: 10.1103/PhysRevLett.105.136102 PACS numbers: 68.03.Fg

During a liquid-vapor phase change process, one of the major issues is the mechanism of energy transport to the interface. Using molecular dynamics, Hołyst and Litniewski [1,2] have reported that, for nanosized droplets, temperature discontinuities can exist at the interface in which the interfacial vapor temperature is greater than the interfacial liquid temperature, and that the evaporation rate is limited by the heat conducted to the interface, but they did not include energy transport by thermocapillary convection in their analysis. Such temperature discontinuities with magnitudes of several degrees have been measured during evaporation at millimeter-sized interfaces [3–5], but similar studies with water and D_2O also indicated that an energy balance could not be obtained unless energy transport by both thermocapillary convection and thermal conduction were included in the analysis [6,7]. This required a new property of water, the surface-thermal capacity c_σ, to be introduced and measured. The reported value of c_σ for H_2O is 30.6 and for D_2O is 32.5 kJ/m^{2}K, and the evaporation studies have reported that thermocapillary energy transport can convey more than 50% of the energy required to evaporate H_2O from the mouth of a stainless steel funnel [6–8]. The value of c_σ can be more rigorously examined using sessile-droplet evaporation because the evaporation flux can be an order of magnitude larger than that from a funnel mouth.

Although sessile-droplet evaporation has received a large amount of attention recently, generally energy transport by thermocapillary convection is being neglected, even though it is being used to promote mixing within droplets [9], to manipulate droplet position [10], and as a source of instability [11]. Further, droplet evaporation is being described by an evaporation model which introduces two fitting functions [12–14], and for the large evaporation rates of millimeter-sized sessile droplets that we consider, the droplets cannot be approximated as spherical caps as considered in [13,15].

We propose a model of sessile-droplet evaporation in which the interfacial temperature discontinuities are taken into account, but no fitting parameters are required. The predictions are examined using an evaporating sessile-water droplet maintained in steady state on an isothermal Cu substrate without buoyancy-driven convection, Fig. 1. The interface was maintained at a constant position by pumping water into the base of the droplet at the same rate as it evaporated at the liquid-vapor interface. During each experiment, the temperatures and the temperature gradients in each phase were measured at 10 positions along the interface. A coupled system of equations was formed that included the statistical rate theory (SRT) expression for the evaporation flux [16–18] and solved to predict the droplet shape and the evaporation rate. These predictions are evaluated by comparing the measured droplet shape and the measured pumping rate with those

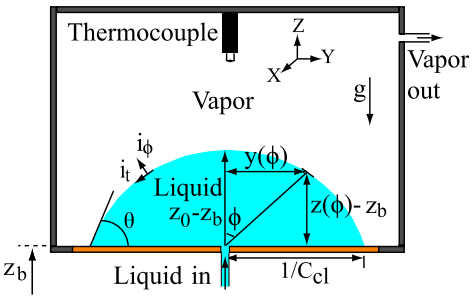

FIG. 1 (color online). In each experiment, an evaporating water droplet with a three-phase-line radius of 9 ± 0.01 mm was maintained on a polished Cu substrate (roughness 53 nm [19]) and in steady state by a syringe pump that injected deionized, degassed water into the droplet base through a small (0.6-mm-diameter) tube at the same rate that vapor was removed from the enclosing chamber. The droplet height and the temperature in the liquid and vapor phases were measured with a U-shaped thermocouple (25 μm bead diameter) that was mounted on a positioning micrometer. The interface height measurements are shown as data points in Fig. 2. The temperature of the Cu substrate was maintained at just below 4 °C, the temperature at which water has its maximum density. The temperature in the liquid at the interface was smaller, due to the evaporation. This decreased the density at the interface below that at the droplet base, eliminating buoyancy-driven convection.

TABLE I. Summary of experiments.

Experiment	EVD1	EVD2	EVD3	EVD4	EVD5
T_0^L (K)	274.33 ± 0.03	275.49 ± 0.03	275.78 ± 0.03	276.14 ± 0.03	276.53 ± 0.03
T_0^V (K)	275.18 ± 0.03	276.23 ± 0.03	276.62 ± 0.03	276.79 ± 0.03	277.30 ± 0.03
C_0^{LV} (m^{-1})	17.5	14.2	19.0	14.7	19.5
$qI(0)$ ($\mathrm{W/m}^2$)	331.6 ± 5	203.5 ± 5	163.8 ± 5	114.3 ± 5	78.4 ± 5
P_0^V (Pa)	658 ± 1	716 ± 1	730 ± 1	751 ± 1	771 ± 1
(y_r, z_r) (mm)	(8, 0.61) ± 0.01	(8, 0.59) ± 0.01	(8, 1.37) ± 0.01	(8, 0.88) ± 0.01	(8, 0.64) ± 0.01
K_p	1.25	1.47	1.58	1.72	1.16
$z_0 - z_b$ (mm)	1.70 ± 0.01	1.57 ± 0.01	2.83 ± 0.01	2.05 ± 0.01	1.81 ± 0.01
θ (rad)	0.672 ± 0.005	0.663 ± 0.005	1.304 ± 0.005	0.946 ± 0.005	0.695 ± 0.005
θ_e (rad)	0.616 ± 0.005	0.569 ± 0.005	1.040 ± 0.005	0.747 ± 0.005	0.658 ± 0.005
$J_{\mathrm{ev}}^{\mathrm{SRT}}$ (mg/s)	0.330 ± 0.001	0.223 ± 0.001	0.173 ± 0.001	0.135 ± 0.001	0.103 ± 0.001
$J_{\mathrm{sp}}^{\mathrm{in}}$ (mg/s)	0.331 ± 0.005	0.223 ± 0.005	0.172 ± 0.005	0.135 ± 0.005	0.103 ± 0.005

predicted. In each experiment, the energy transport by thermal conduction is compared with that by thermocapillary convection. By far the larger portion of energy was transported by thermocapillary convection, but this convection varies strongly over the interface, and is most effective near the three-phase line where most of the evaporation occurs.

If the principal curvatures at a point on the liquid-vapor interface are denoted $C_1^{\mathrm{LV}}(\phi)$ and $C_2^{\mathrm{LV}}(\phi)$, the shape of the droplet may be described in terms of $y(\phi)$ and $z(\phi)$, where ϕ is the turning angle. From differential geometry

$$\frac{dy(\phi)}{d\phi} = \frac{\cos\phi}{C_1^{\mathrm{LV}}}, \qquad \frac{dz(\phi)}{d\phi} = \frac{-\sin\phi}{C_1^{\mathrm{LV}}},$$
$$C_2^{\mathrm{LV}} = \frac{\sin\phi}{y(\phi)}. \tag{1}$$

Since the droplets were axisymmetric, at the apex of each $C_1^{\mathrm{LV}}(0) = C_2^{\mathrm{LV}}(0) \equiv C_0^{\mathrm{LV}}$. If the vapor-phase pressure at the apex is denoted $P_I^V(0)$ and the surface tension of the liquid-vapor interface as γ^{LV}, then from the Laplace equation, the liquid-phase pressure at the apex is given by $P_I^L(0) = P_I^V(0) + 2\gamma^{\mathrm{LV}} C_0^{\mathrm{LV}}$. We suppose the liquid-phase pressure is proportional to the product of the liquid-phase density, the acceleration of gravity, and the depth below the apex, and that $P_I^V(\phi) = P_I^V(0)$. Then we may solve for $C_1^{\mathrm{LV}}(\phi)$:

$$P_I^L[z(\phi)] = P_I^L(0) + K_p(\rho^L g)[z(0) - z(\phi)],$$
$$C_1^{\mathrm{LV}}(\phi) = \frac{P_I^L[z(\phi)] - P_I^V(0)}{\gamma^{LV}} - C_2^{\mathrm{LV}}(\phi). \tag{2}$$

The proportionality factor, K_p, will be determined as a part of the general solution to the governing equations and the boundary conditions.

If the thermal conductivities are denoted as κ^V, κ^L, the unit vector perpendicular to the interface as i_ϕ, the interfacial temperatures in the liquid and vapor phases as $T_I^L(\phi)$ and $T_I^V(\phi)$, then the thermal conduction to the interface, $q_I(\phi)$, is given by

$$q_I(\phi) = (\kappa^V \nabla T^V - \kappa^L \nabla T^L) \cdot i_\phi. \tag{3}$$

Conservation of energy and mass require [6]:

$$j_{ev}(\phi)[h^V(T_I^V(\phi)) - h^L(T_I^L(\phi))]$$
$$= q_I(\phi) - c_\sigma v_t^{lv}\left(\frac{dT_I^L}{dy}\cos\phi - \frac{dT_I^L}{dz}\sin\phi\right), \tag{4}$$

where v_t^{lv} is the fluid speed parallel to the interface, the enthalpies in each phase at the interface are denoted $h^V(T_I^V)$, $h^L(T_I^L)$, the local evaporation flux as $j_{\mathrm{ev}}(\phi)$, and we have neglected viscous dissipation of energy.

Because of symmetry, the thermocapillary convection vanishes at the droplet apex [17,18]. The evaporation flux at this point, $j_{\mathrm{ev}}(0)$, is determined from the measured temperatures and temperature gradients in each phase and Eq. (4). Once $j_{\mathrm{ev}}(0)$ is known, SRT may be applied to express the vapor-phase pressure there in terms of C_0^{LV}. This result may be written symbolically:

$$P_I^V(0) = f_{\mathrm{SRT}}(j_{ev}(0), T_0^L, T_0^V, P^L(0), C_0^{LV}). \tag{5}$$

The curvature C_0^{LV} will act as an iteration parameter to predict the droplet shape. The solution of Eqs. (1)–(5) requires three boundary conditions: at the maximum value of the turing angle ϕ_m, the three-phase-line curvature was measured, C_{cl}, $y(\phi_m)C_{\mathrm{cl}} = 1$ and $z(\phi_m) = z_b$. At $\phi = 0$,

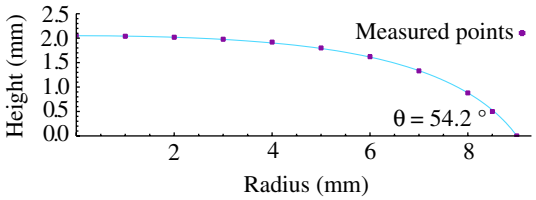

FIG. 2 (color online). A comparison of the measured and predicted liquid-vapor interface profile of experiment EVD4 is shown. The calculated droplet shape is indicated by the solid line. The ±10 μm error bars are within the indicated measurement symbols.

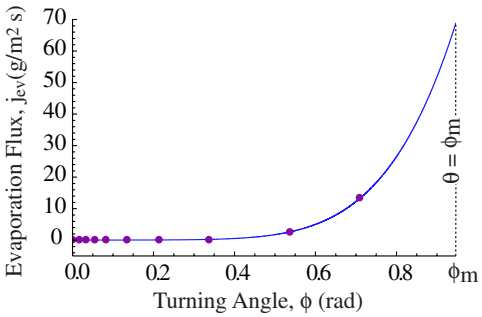

FIG. 3 (color online). The evaporation fluxes determined from SRT at 10 points are shown for experiment EVD4.

$y(0) = 0$ and $z(0) = z_0 - z_b$; the droplet height at y_r was measured, z_r. The values of these parameters for each experiment are listed in Table I.

A double iteration procedure was employed to solve the system of equations. For a chosen value of K_p, the iteration procedure was initiated by choosing a value of C_0^{LV}. Then the system of equations was solved. Once the other boundary conditions were satisfied, the predicted droplet height at y_r was compared with that measured. If this condition was not satisfied, a new value of K_p was chosen and the iteration procedure repeated. The predicted and measured droplet shapes in one experiment are shown in Fig. 2. Once the droplet profile is known, ϕ_m is determined from $z(\phi_m) = z_b$, and the contact angle, θ, from $\theta = \phi_m$, Table I.

If $z(0)$ and C_{cl} are known, but the evaporation ignored, the contact angle of an equivalently sized equilibrium droplet θ_e may be determined by the methods described in [19]. The values of θ_e correlate with θ, but are always less, Table I.

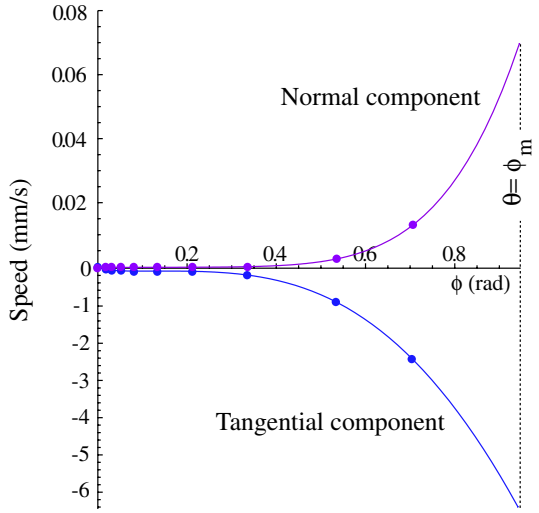

FIG. 4 (color online). In EVD4, the speed parallel to the liquid-vapor interface was in the negative direction: from the three-phase line to the apex. The positive speed perpendicular to the interface indicates evaporation. Note the difference in the negative and positive scales.

The pressures in the liquid and vapor phases at the interface were obtained as part of the procedure to predict the droplet shape, and the temperatures in each phase at 10 points along the interface were measured. This information was used with SRT to predict the evaporation fluxes $j_{\mathrm{ev}}^{\mathrm{SRT}}$ at these points. We emphasize that no fitting parameters were used in these predictions of the evaporation fluxes. The results obtained for experiment EVD4 are shown as solid dots in Fig. 3.

The total evaporation rate was equal to the injection rate of the syringe pump $J_{\mathrm{sp}}^{\mathrm{in}}$ and was used to examine the predicted local evaporation fluxes. These fluxes were fit with a third-order polynomial in $\cos\phi$, the solid line in Fig. 3. This polynomial was integrated over the droplet surface to obtain the predicted total evaporation rate, $J_{\mathrm{ev}}^{\mathrm{SRT}}$. As seen in Table I, there were no measurable differences between $J_{\mathrm{ev}}^{\mathrm{SRT}}$ and $J_{\mathrm{sp}}^{\mathrm{in}}$ in any of these experiments. This indicates conservation of mass was satisfied by the solution to the governing equations and the boundary conditions.

Since the value of c_σ for water has been measured [6,8], and the predicted values of $j_{\mathrm{ev}}^{\mathrm{SRT}}$ at 10 points on the interface has been made, the speed v_t^{lv} at each of these points was determined from conservation of energy, Eq. (4). The values of these speeds for experiment EVD4 are shown in Fig. 4. This speed was negative, meaning its direction was from the three-phase line toward the droplet apex. If the specific volume of the liquid at the interface is denoted $v_f[T_I^L(\phi)]$, the fluid speed perpendicular to the interface, $v_p^{lv}(\phi)$, is given by $v_p^{lv}(\phi) = v_f j_{\mathrm{ev}}(\phi)$. This speed is also given in Fig. 4. The speed parallel to the interface vanishes at the droplet apex, and is thus less than the speed normal to the interface at this point, but at the larger values of ϕ, v_t^{lv} is $\sim 10^2$ times larger than the speed perpendicular to the interface.

Since buoyancy-driven convection was eliminated, the active modes of energy transport were thermal conduction

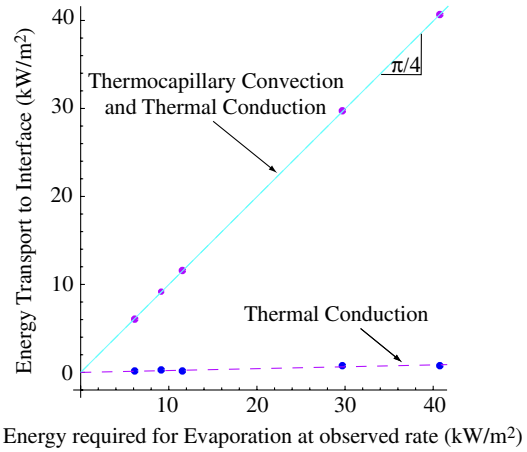

FIG. 5 (color online). If energy transport by both thermal conduction and thermocapillary convection are taken into account, conservation of energy is satisfied, but thermal conduction alone does not satisfy conservation of energy.

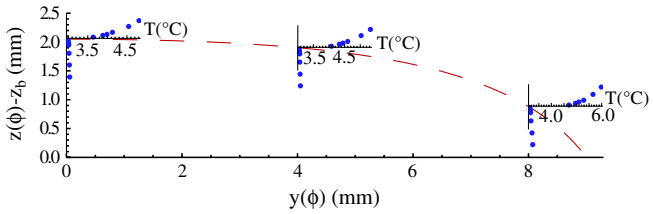

FIG. 6 (color online). The measured temperature profiles at different positions along the interface in the liquid and vapor phases of experiment EVD4 are shown. At the apex, the total heat conducted to the liquid-vapor interface was 114.3 W/m^2 with 59.18% coming from the vapor and the remainder from the liquid. At $\phi = 0.082$, $y(\phi) = 4$ mm, the total increased to 122.8 W/m^2, but that coming from the vapor was reduced to 54.1%. Closer to the three-phase line [$y(\phi) = 8$ mm], the total heat flux increased to 168.3 W/m^2, but the percentage coming from the vapor was reduced to 42%.

and thermocapillary convection. The energy transport by these two mechanisms is compared in Fig. 5. Energy transport by thermocapillary convection was up to 98.4% of that required to evaporate the liquid at the measured rate. However, this mechanism of energy transport varies strongly along the interface. The energy transport by thermal conduction at different positions on the interface is shown in Fig. 6 for experiment EVD4. At the droplet apex, all the energy transported to the interface is by thermal conduction, at $y(\phi) = 4$ mm that by thermal conduction is still 98.5%, but at $y(\phi) = 8$ mm it is only 3.7% of the total. The remainder in each case was by thermocapillary convection. Energy transport by thermocapillary convection is only important near the three-phase line, but there it is dominant, and in this region most of the evaporation occurs. For experiment EVD4, 89.8% of the total evaporation took place for $\phi > 0.55$, Fig. 3, and in this range, thermocapillary convection is the dominant energy transport mode.

These results appear very different from those of Girard *et al.* [20] who interpreted their results for evaporation of small water droplets on an Al substrate as indicating thermocapillary convection was negligible, but some of their assumptions are not consistent with the conditions of our experiments.

We gratefully acknowledge the support of the Natural Sciences and Engineering Research Council of Canada and the Canadian and European Space Agencies.

*charles.ward@utoronto.ca

[1] R. Hołyst and M. Litniewski, Phys. Rev. Lett. **100**, 055701 (2008).
[2] R. Hołyst and M. Litniewski, J. Chem. Phys. **130**, 074707 (2009).
[3] G. Fang and C. A. Ward, Phys. Rev. E **59**, 417 (1999).
[4] G. Fang and C. A. Ward, Phys. Rev. E **59**, 441 (1999).
[5] V. K. Badam, V. Kumar, F. Durst, and K. Danov, Exp. Therm. Fluid. Sci. **32**, 276 (2007).
[6] F. Duan and C. A. Ward, Phys. Rev. E **72**, 056302 (2005).
[7] F. Duan and C. A. Ward, Phys. Rev. E **72**, 056304 (2005).
[8] Fei Duan, V. K. Badam, F. Durst, and C. A. Ward, Phys. Rev. E **72**, 056303 (2005).
[9] M. L. Cordero *et al.*, New J. Phys. **11**, 075033 (2009).
[10] H-B. Nguyen and J-C. Chen, Phys. Fluids **22**, 062102 (2010).
[11] M. F. Schatz and G. P. Neitzel, Annu. Rev. Fluid Mech. **33**, 93 (2001).
[12] R. D. Deegan, O. Bakajin, T. F. Dupont, G. Huber, S. R. Nagel, and T. A. Witten, Nature (London) **389**, 827 (1997).
[13] H. Hu and R. G. Larson, J. Phys. Chem. B **106**, 1334 (2002).
[14] W. D. Ristenpart, P. G. Kim, C. Domingues, J. Wan, and H. A. Stone, Phys. Rev. Lett. **99**, 234502 (2007).
[15] F. Girard, M. Antoni, and K. Sefiane, Langmuir **26**, 4576 (2010).
[16] C. A. Ward and G. Fang, Phys. Rev. E **59**, 429 (1999).
[17] Fei Duan, Ian Thompson, and C. A. Ward, J. Phys. Chem. B **112**, 8605 (2008).
[18] A. H. Persad and C. A. Ward, J. Phys. Chem. B **114**, 6107 (2010).
[19] H. Ghasemi and C. A. Ward, J. Phys. Chem. C **114**, 5088 (2010).
[20] F. Girard, M. Antoni, and K. Sefiane, Langmuir **24**, 9207 (2008).